DOI: 10.1002/cbic.200800510

Stable Long-Term Intracellular Labelling with Fluorescently Tagged Cationic Magnetoliposomes

Stefaan J. H. Soenen,[a] Dries Vercauteren,[b] Kevin Braeckmans,[b] Wim Noppe,[a] Stefaan De Smedt,[b] and Marcel De Cuyper*[a]

Iron oxide nanocrystals that are dextran coated are widely exploited biomedically for magnetic resonance imaging (MRI), hyperthermia cancer treatment and drug or gene delivery. In this study, the use of an alternative coating consisting of a phospholipid bilayer directly attached to the magnetite core is described. The flexible nature of the magnetoliposome (ML) coat, together with the simple production procedure, allows rapid and easy modification of the coating, offering many exciting possibilities for the use of these particles in biomedical applications. Upon incubation of neutral MLs with an equimolar amount of cationic 1,2-distearoyl-3-trimethylammoniumpropane (DSTAP)-bearing vesicles, approximately one third of the cationic lipids are incorporated into the ML coat. This is in line with a theoretical model predicting transferability of only the outer leaflet phospholipids of bilayer structures. Most interestingly, the use of MLs containing 3.33% DSTAP with a positive ζ-potential of (31.3 ± 7.3) mV (mean ± SD) at neutral pH, results in very heavy labelling of a variety of biological cells (up to (70.39 ± 4.52) pg of Fe per cell, depending on the cell type) without cytotoxic effects. The results suggest the general applicability of these bionanocolloids for cell labelling. Mechanistically, the nanoparticles are primarily taken up by clathrin-mediated endocytosis and follow the endosomal pathway. The fate of the ML coat after internalisation has been studied with different fluorescent lipid conjugates, which because of the unique features of the ML coat can be differentially incorporated in either the inner or the outer layer of the ML bilayer. It is shown that, ultimately, iron oxide cores surrounded by an intact lipid bilayer appear in endosomal structures. Once internalised, MLs are not actively exocytosed and remain within the cell. The lack of exocytosis and the very high initial loading of the cells by MLs result in a highly persistent label, which can be detected, even in highly proliferative 3T3 fibroblasts, for up to at least one month (equivalent to approximately 30 cell doublings), which by far exceeds any values reported in the literature.

Introduction

Over the last two decades, magnetisable iron oxide nanocrystals have been increasingly exploited as vectors for efficient gene delivery,[1] mediators of hyperthermia cancer treatment[2] or magnetic resonance imaging (MRI) contrast agents.[3] For MRI purposes, iron oxide cores are commonly used as so-called T_2 contrast agents and can be divided into either superparamagnetic iron oxides (SPIOs), with diameters of >50 nm, or ultrasmall SPIOs (USPIOs), with diameters of <50 nm.[4] For purposes of cell labelling, a high internalisation efficiency of the iron oxide core is desirable, and detailed knowledge of the behaviour of the contrast agent in a cellular environment is indispensable.

A prerequisite for the elaboration of successful applications is that the particles must be stable. This can be achieved by addition of a protective coating around the particles; this results in a so-called core-corona structure.[5] A wide variety of substances can be used as coating material; these include synthetic[3a,4] or natural (for example, dextran[6b,7] or proteins[8]) polymers and amphiphilic molecules such as fatty acids[9] or phospholipids.[10] For MRI purposes, the most common type of coating consists of dextrans; these particles, however, can elicit allergic reactions when used in vivo,[11] and in addition they are not well suited for chemical derivatisation, because the weakly physisorbed molecules are slowly lost during chemical manipulations.[5,12] Such derivatisations would, however, greatly enhance the applicability of nanocrystals; surface grafting of cell-penetrating peptides, such as penetratin, or the TAT peptide, for example, can significantly increase cellular uptake,[13] and ligands that specifically target cellular receptors can provide a means of tissue-specific delivery of (U)SPIOs.[6b,14] With regard to the use of nanocrystals as MRI contrast agents, these dextran-coated iron oxide formulations currently require the addition of transfection agents to achieve substantial uptake levels,[7,15] which possibly induce cell toxicity.[16] Moreover, the way in which particles loaded with transfection agent interact with cells is often only poorly addressed, leaving many unanswered questions.

One promising alternative to dextran-coated SPIOs is the use of phospholipid-coated USPIOs—so-called magnetolipo-

[a] MSc. S. J. H. Soenen, Dr. W. Noppe, Prof. M. De Cuyper
Subfaculty of Medicine, Katholieke Universiteit Leuven
Interdisciplinary Research Centre, KUL-Campus Kortrijk
E. Sabbelaan 53, 8500 Kortrijk (Belgium)
Fax: (+32) 56-246997
E-mail: marcel.decuyper@kuleuven-kortrijk.be

[b] MSc. D. Vercauteren, Dr. K. Braeckmans, Prof.. S. De Smedt
Faculty of Pharmaceutical Sciences, University of Gent
Harelbekestraat 72, 9000 Gent (Belgium)

Supporting information for this article is available on the WWW under http://dx.doi.org/10.1002/cbic.200800510

somes (MLs). Because phospholipids are naturally occurring substances, these MLs exhibit superb biocompatibility.[17] The MLs originally developed in our laboratory consist of iron oxide cores each wrapped in a phospholipid double layer, to give complete encapsulation of the iron oxide. The inner layer of such a phospholipid bilayer is strongly chemisorbed onto the iron oxide core, while the outer layer is more loosely physisorbed; this allows exchange of these (phospho)lipids with those in vesicles incubated with the MLs.[18] Functionalised MLs are therefore easily generated by incubation of the MLs with vesicles containing the functional groups, such as (activated) poly(ethylene glycol) chains or chelating moieties, attached to phospholipids by appropriate chemical coupling.[19] By simply varying the content of the functionalised lipids in the donor vesicles or working with an appropriate donor vesicle/acceptor ML ratio, the concentration of functionalised lipid, such as cationic lipid, in the ML bilayer can be easily modulated.

In this work, the architecture of the lipid coat of cationic MLs was investigated. Next, different cell types were mixed with MLs containing 3.33% 1,2-distearoyl-3-trimethylammoniumpropane (DSTAP, 100 μg of Fe per mL), and uptake levels and cell viability were examined. With 3T3 fibroblasts as a representative cell model, this study was extended by examining the effect of a broader range of ML concentrations (50–500 μg of Fe per mL). The route by which MLs were taken up was examined, and the cellular localisations of all the components of the ML (iron oxide core and both the inner and outer phospholipid layers of the coating material) were determined. The stability of the label was tested with regard to possible exocytosis, together with the persistence of the ML label during the dilution that is due to continuous cell proliferation. The results showed that the MLs are very robust and promising tools for the clinical detection and therapy of malignant tissues.

Results

Cationic ML characterisation

Transmission electron micrographs of the magnetic fluid stock solution used to produce MLs showed an average nanoparticle diameter of (14.0 ± 0.3) nm.[20] To produce cationic MLs, dipalmitoylphosphatidylcholine (DPPC) acceptor MLs were incubated at an equimolar lipid concentration with donor vesicles consisting of DSTAP (20%) and dimyristoylphosphatidylcholine (DMPC, 80%). The amount of each type of fatty acyl chain in the ML coat was quantified by gas-liquid chromatography (Table 1). The data showed that equilibrium was reached within the first day, at which time approximately one third of the original amount of vesicle-derived lipid was incorporated into the ML bilayer.

Table 1. Percentages of DPPC, DMPC and DSTAP in the ML coat as derived from gas–liquid chromatograms.

	Presence in ML coat at:		
	0 h	1 h	24 h
DPPC	100%	66.90 ± 2.42%	63.57 ± 3.28%
DMPC	0%	26.77 ± 1.45%	29.44 ± 2.25%
DSTAP	0%	6.33 ± 0.34%	6.99 ± 0.30%

On incubation of DSTAP-containing MLs with cells, MLs containing 3.33% DSTAP were found to give optimal results in terms of labelling and the absence of cytotoxicity.[20] This type of ML was therefore regarded as the "gold standard" for investigation of ML–cell interactions in subsequent experiments. Transmission electron miscroscopy (TEM) of MLs containing 3.33% DSTAP showed electron-dense iron oxide cores each surrounded by a phospholipid bilayer, visualised by negative staining with uranyl acetate (Figure 1). Further analysis indicated an average ML diameter of (21 ± 1.3) nm, which signifies a thickness for the lipid double layer of approximately 3.5 nm. The ζ-potential of these particles at pH 7.0 (5 mM TES buffer) was (31.3 ± 7.3) mV (mean ± SD).

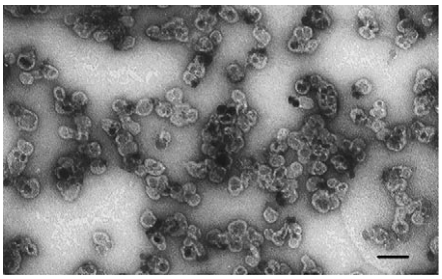

Figure 1. Transmission electron micrograph of MLs containing 3.33% DSTAP. The phospholipid bilayer is negatively stained with uranyl acetate; scale bar: 40 nm.

Incubation of MLs containing 3.33% DSTAP with various cell types

To examine whether the MLs were efficiently taken up by a variety of cell types, MLs containing 3.33% DSTAP (concentration 100 μg Fe per mL) were incubated with 3T3 fibroblasts, N2a neuroblastoma cells, HEK-293 (human embryonic kidney) cells, Geneswitch™-CHO (Chinese hamster ovary) cells or HUVECs (human umbilical vein endothelial cells). The iron content per cell of cells incubated with these MLs for 4 or 24 h is shown in Figure 2A. The data showed some variability in uptake efficiency between different cell types; this indicates cell-type dependent internalisation efficiency. No cytotoxic effects were noted with any of the cell types tested (Figure S1 in the Supporting Information).

Using 3T3 fibroblasts as a standard cell model, we tested cellular uptake efficiency with MLs at various concentrations (50–500 μg of Fe per mL). The data for an incubation period of 4 h are shown in Figure 2B. The cells were found to display saturable uptake efficiency, and the increment in iron uptake decreased as the ML concentration increased. Increasing the ML concentration did not have any effect on cellular viability measured after 4 and 24 h (Figure S2 in the Supporting Information).

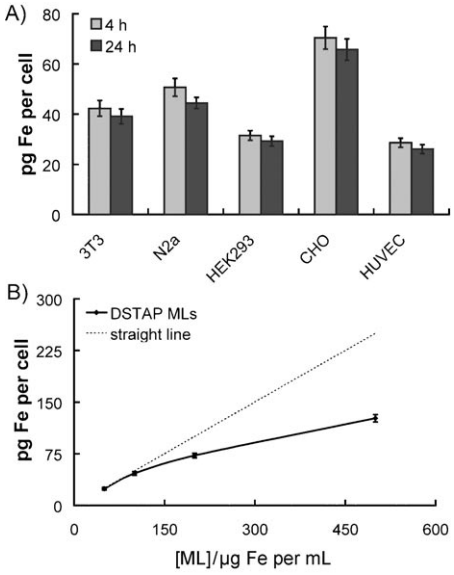

Figure 2. Iron content (pg Fe per cell) of A) different cell types (3T3 fibroblasts, N2a neuroblastoma cells, HEK-293 cells, Geneswitch™-CHO cells and primary HUVECs) incubated for 4 or 24 h with MLs containing 3.33% DSTAP, or B) of 3T3 fibroblasts incubated for 4 h with different concentrations (50, 100, 200 and 500 µg Fe per mL) of MLs containing 3.33% DSTAP. The error bars indicate the mean ± SEM ($n = 10$), the straight line depicts a linear relationship between ML concentration and cellular iron content.

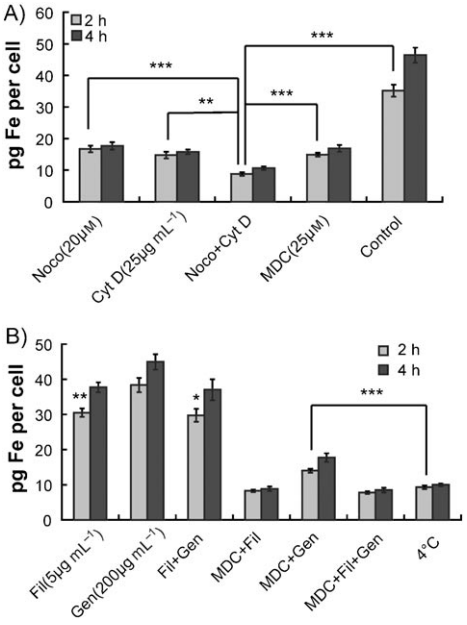

Figure 3. Iron content (pg Fe per cell) of 3T3 fibroblasts incubated for 2 or 4 h with MLs containing 3.33% DSTAP in the presence of various endocytosis inhibitors (Noco, Cyt D, Fil, Gen and MDC and mixtures) or in the absence of any inhibitors at 37 °C (control cells) or 4 °C. The error bars indicate the mean ± SEM ($n = 10$), and the degree of significance of differences between two setups is indicated. A) Noco+Cyt D in relation to the other setups; B) Fil, Gen, Fil+Gen in relation to control cells; MDC+Fil, MDC+Gen, MDC+Fil+Gen in relation to uptake at 4 °C; *: $p < 0.05$; **: $p < 0.01$; ***: $p < 0.001$.

Route of ML uptake

The saturable increase in uptake levels suggested a clathrin-mediated endocytosis route for the MLs (see the Discussion). To clarify the mechanism of ML internalisation, MLs containing 3.33% DSTAP were incubated with cells treated with various types of endocytosis inhibitor. Both nocodazole (Noco), which destabilises microtubules, and cytochalasin D (Cyt D), which depolymerises actin microfilaments, unspecifically inhibit several endocytosis pathways. Filipin III (Fil) is a sterol-binding agent that removes cholesterol from the plasma membrane, and thus affects multiple endocytotic pathways. Monodansyl cadaverine (MDC) specifically inhibits clathrin-mediated endocytosis, whereas genistein (Gen) specifically inhibits caveolin-mediated endocytosis. The optimal concentration of each type of inhibitor was evaluated to maximise its efficiency and to rule out any toxic side effects. Figure 3 shows the iron uptake per cell for the selected conditions, as well as data for combinations of several inhibitors at the selected concentrations and the results for 3T3 fibroblasts incubated with MLs containing 3.33% DSTAP in the absence of inhibitors (controls) at 4 °C. The results are shown for incubation periods of 2 and 4 h.

All inhibitors except Gen significantly reduced the uptake efficiencies of MLs (Figure 3) when no sign of cytotoxicity was observed (data not shown). Noco and Cyt D, which affect both the clathrin-dependent and clathrin-independent pathways, inhibited endocytosis to the same extents (at 4 h, uptakes were (38.09 ± 1.18) and (34.02 ± 0.76)%, respectively, of control levels). A combination of the two compounds reduced uptake to about (22.96 ± 0.56)% of control levels; this is equal to the level seen when cells were incubated at 4 °C and probably indicates complete cessation of endocytosis. The remaining "uptake" was probably due to MLs attached to the cell surface and not removed by the washing steps. The use of the clathrin-mediated endocytosis inhibitor MDC or the unspecific inhibitor Fil reduced uptakes to (36.42 ± 1.06) and (80.13 ± 1.41)%, respectively, of control values, whereas when combined they led to only (21.73 ± 0.66)% uptake; this indicates the complementary action of these inhibitors and suggests that MLs are taken up by different routes, but primarily through unspecific receptor binding and subsequent clathrin-mediated endocytosis.

Intracellular localisation of cationic MLs

The above results suggested that MLs were primarily taken up by clathrin-mediated endocytosis, resulting in their localisation in intracellular endosomal compartments. TEM micrographs of 3T3 fibroblasts incubated with MLs containing 3.33% DSTAP (100 µg Fe per mL) for 24 h supported this hypothesis; the cells showed heavily labelled endosomal structures as well as noninternalised MLs that adhered to the plasma membrane (Figure 4). As TEM only allows visualisation of the magnetite core, and not the lipid bilayer when used in a cellular environment, the fate of the ML coat during internalisation remained unknown. In order to determine whether the lipids were to be found in endosomal structures, we produced asymmetric MLs containing 3.33% DSTAP, in which the inner layer was labelled with β-BODIPY® FL C_5-HPC (1%), whereas the outer layer was

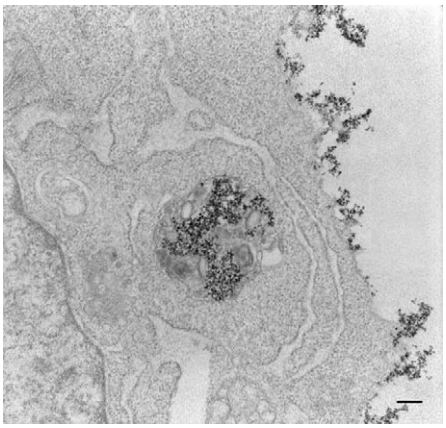

Figure 4. Transmission electron microscopy of ML internalisation by fibroblasts; this provides visual confirmation that MLs containing 3.33% DSTAP were internalised and were found in endosomal structures located near the cell nucleus; scale bar: 150 nm.

either unlabeled or labelled with DPPE-Lissamine™ Rhodamine B (0.1%, see the Experimental Section). The unifluorescent MLs (100 μg Fe per mL) were incubated with 3T3 fibroblasts, after which fresh medium containing Lysotracker Red (60 nM) was incubated with the cells for 1 h, and colocalisation of the endosomal compartments and the inner ML layer was then examined by confocal microscopy (Figure 5).

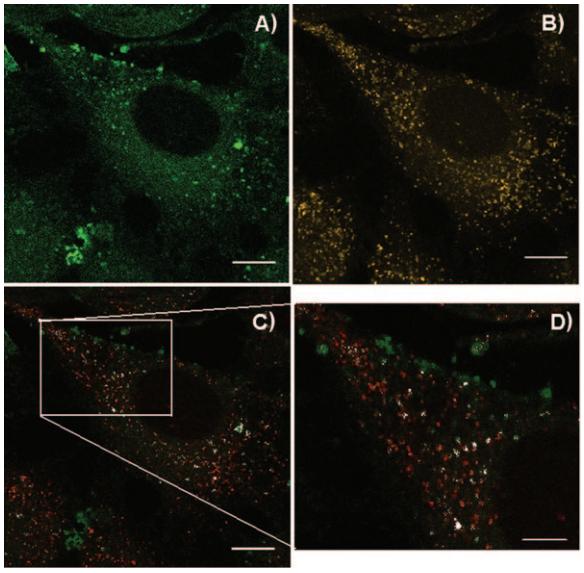

Figure 5. Confocal images of 3T3 fibroblasts incubated for 4 h with A) β-BODIPY FL C_5-HPC labelled (1%) MLs containing 3.33% DSTAP. B) Lysosomes were stained with Lysotracker Red (60 nM) and the cells were fixed. C) Colocalisation (white) was analysed by use of ImageJ software. D) An enlargement of the section indicated in (C). The scale bars are either 10 μm (A–C) or 4 μm (D).

Figure 5A shows heavy labelling of the cell with the unifluorescent MLs. The endosomal compartments (Figure 5B) were spread evenly throughout the cytoplasm and seemed to colocalise with the majority of the internalised MLs (Figure 5C, white spots). The enlarged section clearly shows a high degree of colocalisation (Figure 5D), and all the internalised MLs are present in endosomal structures. MLs not taken up are seen as green regions on the plasma membrane (Figure 5D). The 3T3 fibroblasts were first incubated with bifluorescent MLs (100 μg Fe per mL) and then in ML-free medium for 48 h, after which time the cells were washed with PBS and fixed; colocalisation of the inner and outer layers of the ML coat was investigated by confocal microscopy. A representative image showing both the inner (green) and outer lipid layers (yellow) is shown in Figure S3; there is a high degree of colocalisation (white) of these lipid layers after cell internalisation.

Examination of particle exocytosis

It is important to know whether internalised particles remain inside the cell or are released. The clathrin-mediated route of uptake suggests that they were possibly exocytosed through the formation of so-called recycling endosomes. To investigate this, MLs containing 3.33% DSTAP and labelled in the outer lipid layer with DPPE-Lissamine™ Rhodamine B (0.25%) were incubated with 3T3 fibroblasts for 4 h, the medium was then removed, and fresh medium not containing MLs was added to the cells, which were fixed at different times and examined by fluorescence microscopy. At each time point, eight samples were treated as described above, and four of these were subjected to an additional incubation step (5 min) with trypan blue (0.4%, *w/v*) prior to being fixed. This step quenches extracellular fluorescence and leaves only the fluorescence of internalised particles.[21] With this method it is possible to investigate the loss either of intracellular or of total (intracellular + adhering) MLs. The relative fluorescence of the samples was investigated with the aid of ImageJ software, and sample pictures for every time point are shown in Figure 6 (A–J: without trypan blue; K–T: with trypan blue), together with the fluorescence intensity (arbitrary units) as a function of time for both sets of conditions (Figure 6U, 6V, respectively). The data show no dilution of particles over the time period investigated for either the total or purely intracellular fluorescence. In fact, in the cells treated with trypan blue as a quencher dye, the relative fluorescence increased, rather than decreased.

Particle retention

Earlier results had indicated dilution of labelled MLs in growing cells over time.[20] As the MLs in our study were not actively exocytosed, it is highly probable that this dilution was due to the continuous expansion of the cell population, as 3T3 fibroblasts have a short doubling time. To test this hypothesis, cells were treated with tubulin polymerisation inhibitor II (TPI), which has a strong antiproliferative effect. Different concentrations of TPI were tested on 3T3 fibroblasts to find the optimal conditions (that is, the lowest concentration with high efficacy; data not shown). A small portion of the cells died due to TPI treatment, but the number of remaining cells remained constant and the cells were completely viable as determined by the MTT assay (data not shown). In practice, cells were treated

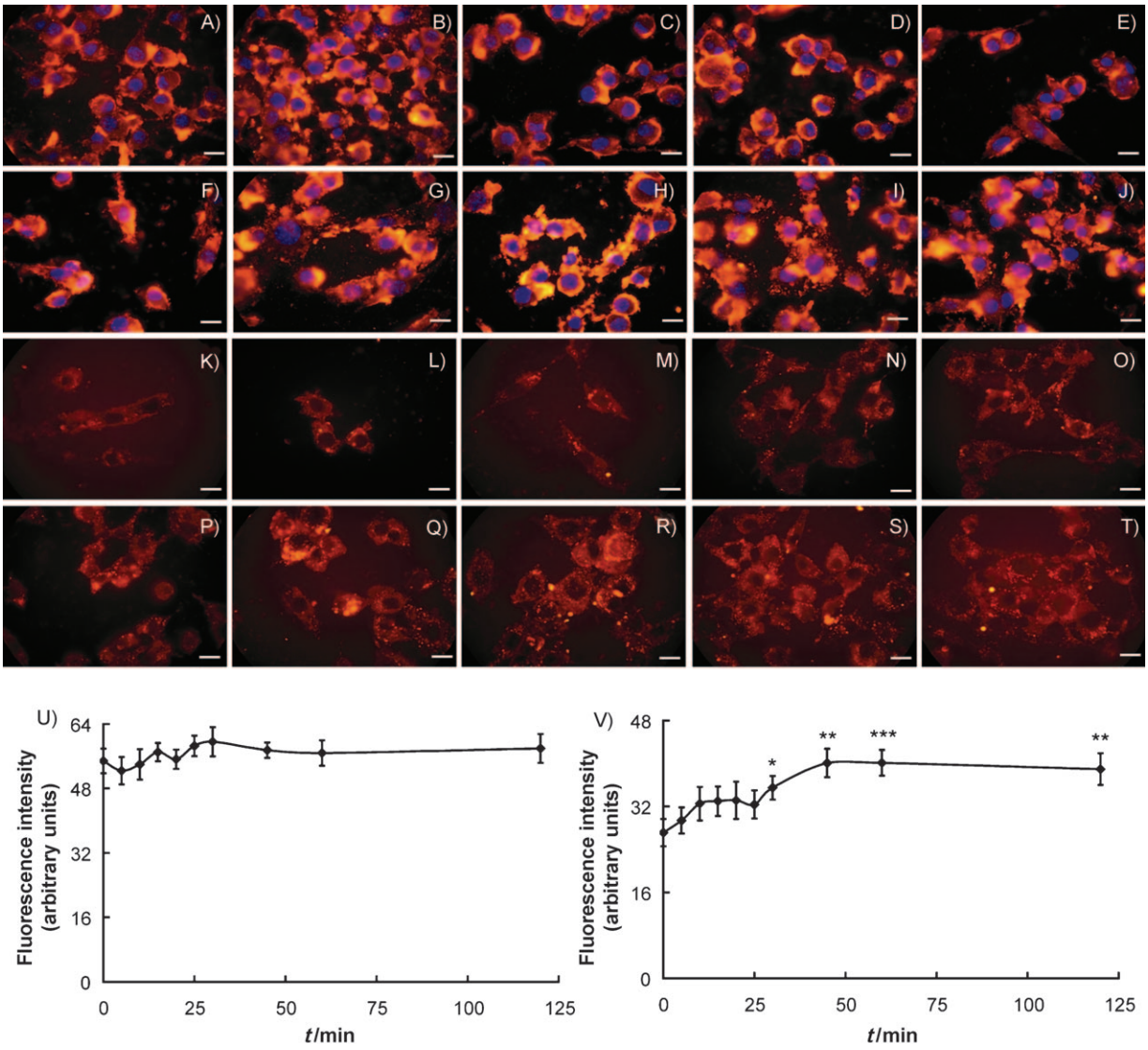

Figure 6. Fluorescent micrographs of 3T3 fibroblasts (blue colour: DAPI nuclear staining) incubated for 4 h with MLs containing 3.33% DSTAP, labelled with DPPE-Lissamine™ Rhodamine B (0.25%, red colour), after which the medium was replaced with fresh medium without MLs, and samples were taken immediately (A, K) or after 5 (B, L), 10 (C, M), 15 (D, N), 20 (E, O), 25 (F, P), 30 (G, Q), 45 (H, R), 60 (I, S), 120 (J, T) minutes of incubation. U) and V) The relative fluorescence intensities versus incubation time for samples corresponding either to A)–J), which are normally treated cells, or to K)–T), which are trypan blue (0.4%) treated cells, respectively. The error bars indicate the mean ± SEM ($n = 40$) and the degree of significance is shown relative to the intensity at time point 0.

with TPI (1 μM) and incubated for 24 h, after which time the medium and any dead cells were removed, and the viable cells were then incubated with MLs containing DSTAP (0, 1.66, 3.33, 6.66 or 16.66%) at the same concentration (100 μg Fe per mL), because dilution of the particles is clearer at higher uptake levels. Cell viability (data not shown) and iron content were then determined at different time points.

The results in Figure 7A show a slow time-dependent decrease in the iron oxide content for cells treated with normal control medium, which is compatible with a model of dilution of the particles due to continuous expansion of the cell population. As shown in Figure 7B, treatment of the cells with TPI led to a lower maximal uptake for each type of particle, but also reduced or even completely halted the time-dependent decrease in the average cellular ML content; this led to much better retention of MLs in the cell. Uptake could be divided into two main stages: continuous uptake, which reached a maximum at about 8 h, followed by a steady-state level, in which the cells seemed saturated with MLs. The levels of saturation were determined by the amount of cationic lipid present in the ML coat.

Long-term persistence of the ML label

As stated above, the short doubling time of 3T3 fibroblasts leads to dilution of the MLs. To allow for continued in vivo detection of cells by MRI or to ensure high enough doses of MLs for hyperthermia treatment after several rounds of cell division, it is important to determine the retention of MLs within highly proliferative cells. To this end, a batch of 3T3 fibroblasts were

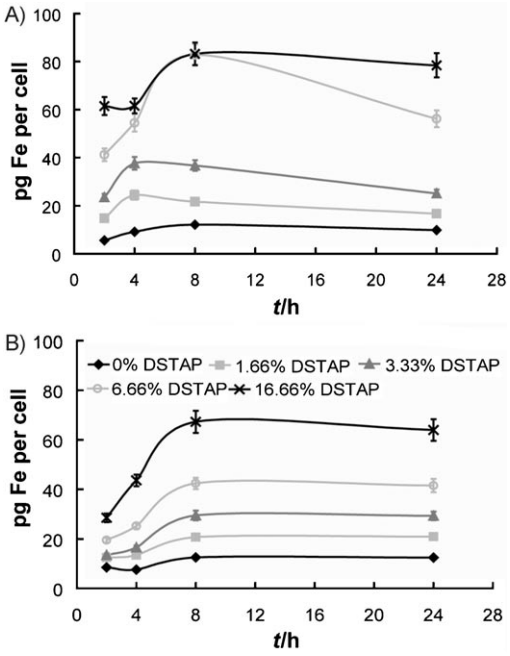

Figure 7. Iron content (pg Fe per cell) of 3T3 fibroblasts incubated for 2, 4, 8 or 24 h with MLs containing DSTAP (0, 1.66, 3.33, 6.66 or 16.66%) in A) the absence, or B) the presence of TPI (1 μM), which creates a stable, nondividing cell population. The error bars indicate the mean ± SEM ($n = 10$).

incubated for 24 h with MLs containing 3.33% DSTAP labelled with DPPE-Texas Red® (0.25%, 100 μg Fe per mL); the cells were thereafter placed in fresh medium without MLs and cultured for different time periods, after which samples were plated out, fixed and checked for ML presence by fluorescence microscopy.

The data presented in Figure 8 clearly show attenuation of the fluorescent signal; this signifies a dilution of the MLs over time. However, the fluorescent biocolloids could still be detected for up to at least one month by fluorescence microscopy; this indicates strong and persistent labelling.

Discussion

The MLs used in this work displayed several key characteristics for use in a wide variety of biomedical applications, such as MRI, hyperthermia treatment or (intracellular) drug delivery.[4,5,6b] The superior features of these MLs are due to their coating, which consists of a lipid bilayer that is very strongly chemisorbed to the iron oxide core. In general, to cover the iron oxide core with the lipid bilayer, lauric acid-stabilised iron oxide cores are dialysed in the presence of phospholipids. During this process, lauric acid molecules are replaced by lipid molecules, which leave the donor vesicles, travel through the aqueous phase and are taken up by the acceptor MLs; this follows the kinetics of the so-called "aqueous transfer model".[22] The inner lipid layer is constructed according to a high-affinity adsorption regime, whereas formation of the outer lipid layer obeys Langmuir adsorption mathematics and is driven by the hydrophobic effect.[23]

The production of cationic MLs requires two consecutive steps: the formation of neutral MLs, followed by incubation with cationic vesicles (see the Experimental Section). Taking into account the fact that for 20 nm diameter vesicles two thirds of the lipids are present in the outer lipid layer, and assuming that during ML production only the outer layer lipids participate in the exchange process, one can theoretically deduce that upon incubation of neutral MLs with an equimolar amount of cationic vesicles, equilibrium will be reached when the MLs contain one third of the amount of cationic lipid originally present in the donor vesicles.[18] The data in Table 1 confirmed this, as approximately one third of the amount of lipids present in the ML coat was derived from the vesicles, and also showed that this ratio of vesicle-derived lipids to ML-derived lipids is rapidly achieved and maintained for at least 24 h. This finding further strengthens the suggestion that intramembrane flip-flop movements, which are thermodynamically unfavourable, are very slow (half-lives of several days) and do not occur within the time-span investigated.[20,24]

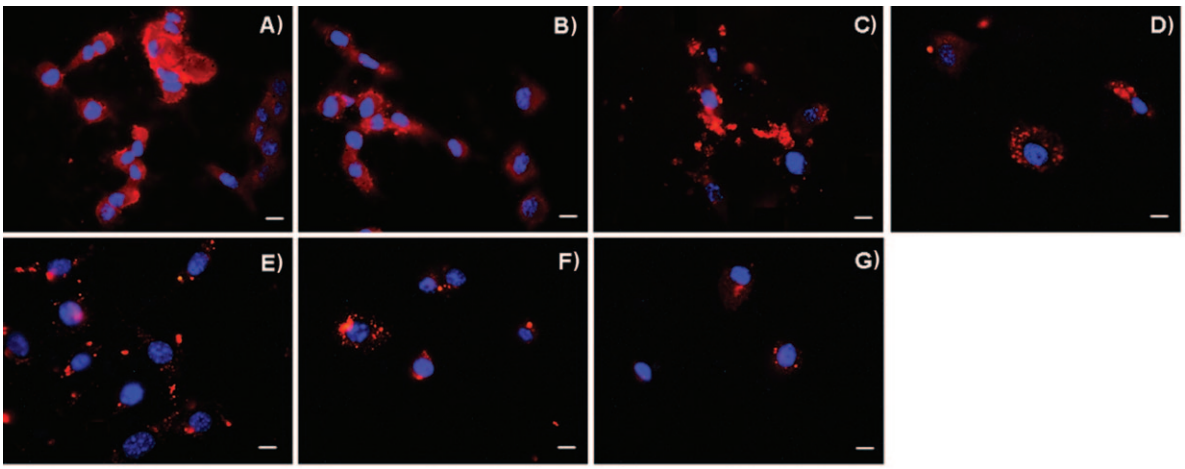

Figure 8. Fluorescence micrographs of 3T3 fibroblasts incubated for 24 h with MLs containing 3.33% DSTAP and labelled with Texas Red (0.25%, red). Nuclei were stained with DAPI (blue). Images were taken of cells cultured in medium not containing any MLs at A) 0, B) 2, C) 5, D) 10, E) 20, F) 25 or G) 30 days post-ML incubation; scale bars = 25 μm.

These features were exploited to prepare MLs in which the lipid bilayer was labelled with different fluorophores (Scheme 1); this provided further insight into the fate of the lipid bilayer after internalisation (see below). To label the inner layer, we chose to use a lipid with a fluorescent tag located at the end of a truncated fatty acyl chain, as this configuration will not hinder the strong anchoring of the phospholipids on the iron oxide surface. In contrast, to label the outer layer, we preferred to work with the fluorescent moiety in the polar head-group region so that it could freely protrude into the surrounding medium. Thus, practically, β-BODIPY FL C_5-HPC was used to monitor the inner lipid layer and DPPE-Lissamine™ Rhodamine B or DPPE-Texas Red were used to label the outer leaflet of the ML bilayer.

The results presented in Figure 2A showed that MLs containing 3.33% DSTAP can be regarded as a universal particle that can be employed to label many different cell types efficiently and safely. The variation in iron levels seems to depend upon the general transfection efficacies of the cell types used. Internalisation was lowest with HUVECs, which are primary cells known to be rather resistant to conventional transfection protocols,[25] but in our hands still reached an impressive (28.63 ± 1.83) pg of iron per cell after 4 h incubation, which is significantly higher than the uptake levels reported to date with, for instance, dextran-coated particles in combination with transfection agents.[26] The highest uptake was seen with GeneSwitch™-CHO cells ((70.39 ± 4.52) pg Fe per cell after 4 h), which are generally considered to be easily transfected. Figure 2B shows that the increase in uptake efficiency at higher ML concentrations was saturable, as the increase in cellular iron levels deviates more from a linear relationship at higher iron levels in the medium, which is indicative of unspecific receptor-mediated endocytosis.[27]

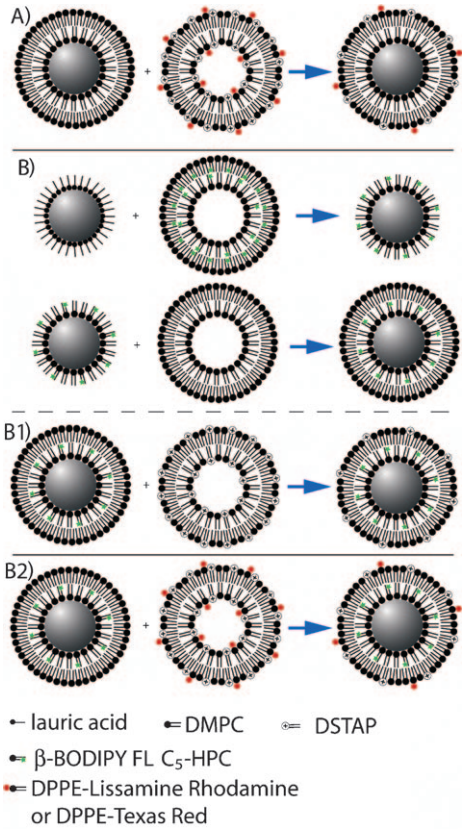

Scheme 1. A simplified scheme depicting the production of different types of fluorescently tagged MLs. A) Cationic MLs with tagged outer lipid layer, B) neutral MLs with tagged inner lipid layer—B1) cationic MLs with tagged inner lipid layer, B2) cationic MLs with differently tagged inner and outer lipid layers. For the experimental details, see the Experimental Section.

To clarify the route of uptake, several endocytosis inhibitors were tested for efficacy in inhibition of ML uptake (Figure 3). The unspecific inhibitors Cyt D, which depolymerises actin microfilaments, and Noco, which destabilises microtubules,[28] both greatly inhibited uptake, and their effect could be increased by combining them, which resulted in the inhibition of most transcytosis and movement of endosomes. Uptake was reduced to (22.96 ± 0.56)% of control levels, almost identical to the (22.18 ± 0.39)% obtained when incubation was at 4 °C, and no active endocytosis occurred. This shows that over 2–4 h of incubation, approximately 22% of the cell-associated MLs were bound to the plasma membrane, while the remaining 78% were internalised. Several specific inhibitors were then used to determine the actual pathway followed during internalisation. MDC is a competitive inhibitor of transglutaminase, which is an enzyme essential for the formation of clathrin-coated vesicles;[29] Fil removes cholesterol from the plasma membrane, and thus disturbs several internalisation pathways; and Gen is a specific inhibitor of caveolae-mediated endocytosis.[28] As Gen had no effect on ML uptake, caveolae-mediated endocytosis does not seem to play a role. If the amount of internalised MLs is solely considered, MDC inhibited uptake by (83.13 ± 1.56)%, whereas Fil resulted in (25.71 ± 1.22)% inhibition, and both together reduced uptake efficiency to the level seen at 4 °C; this indicates that Fil has a complementary effect (15% inhibition) to MDC, but also acts on the same pathway as MDC, as alone it caused 25% inhibition. By removing cholesterol from the plasma membrane, Fil strongly inhibits several pathways, such as macropinocytosis and caveolin-mediated endocytosis, and also partially affects clathrin-mediated endocytosis, as lack of cholesterol diminishes the potential of coated pits to detach from the plasma membrane.[30] This last effect would explain the partial overlapping effect of MDC and Fil. The secondary internalisation route is probably macropinocytosis, as cholesterol plays a role in macropinosome formation.[28] This suggestion is supported by the inhibitory effect of Cyt D being greater than that of MDC, suggesting involvement of the actin cytoskeleton, as Cyt D reduces membrane ruffling. Taken together, these findings show that MLs are internalised primarily by clathrin-mediated endocytosis, (85.31 ± 1.72)%. This is in agreement with the results of Rejman et al.,[31] who found that the precise route of particle uptake is size-dependent, with particles smaller than 200 nm diameter being internalised by clathrin-mediated endocytosis.

As clathrin-mediated endocytosis targets particles to the endosomal pathway, we hypothesised that MLs would end up in endosomal structures. TEM micrographs (Figure 4) showed deposition of the MLs in endosomal structures located close to

the cell nucleus, as seen with several types of internalised (U)SPIOs.[3a,32] The intracellular localisation of the lipid bilayer can be visualised, as the flexible ML coat can easily be tagged with a fluorescent label to produce a bimodal contrast agent. Figure 5 shows that although many endosomal structures did not contain any MLs, all the internalised MLs seemed to colocalise to a high degree with Lysotracker Red (Figure 5C and D), which testifies to a lysosomal localisation of the lipid coat, in addition to the iron oxide core. Green dots were seen only at the cell peripheries and indicate adherent MLs that had not been internalised; these correspond to the 22% of particles that stuck to the membranes of the cells even after complete inhibition of endocytosis. Figure S3 in the Supporting Information also shows a high degree of colocalisation of the inner and outer lipid layers, which clearly shows that, during the process of internalisation, the more loosely bound outer lipid layer of the MLs stays intact and does not, for instance, fuse with the plasma membrane.

Exocytosis of particles in serum-containing media has been demonstrated in many studies;[15,27,28] it can have a negative effect on the stability of the label over time and can also lead to labelling of nontarget cells if particles are released into the surrounding tissue from prelabelled transplanted cells. Possible exocytosis of our particles was investigated by fluorescence microscopy. In the presence of trypan blue, specific quenching of all extracellular fluorescence occurred;[21] this allowed the visualisation only of intracellular MLs, whereas in the absence of trypan blue total fluorescence was seen. Combining these two methods allowed us to investigate the loss of internalised particles or of particles adherent to the cell surface. Figure 6A–J and 6U show no change in total fluorescence, whereas Figure 6K–T and 6V show that the amounts of internalised MLs increased—rather than decreased—over time. This can be explained as a result of continuous internalisation of MLs adherent to the surface, even after removal of the ML-containing medium. As the use of trypan blue reduced the intensity of the fluorescent signal (as shown by the very weak DAPI signal), it was not possible to determine the ratio of internalised particles to total cell-associated particles, because the signal intensity of internalised particles is significantly weakened. The findings reported thus far also indicate the need for more cautious determination of cellular iron contents, as most studies that report on cellular iron contents do not use methods that can discriminate between internalised and adherent particles. As such, the amount of particles should be defined as "cell-associated particles" and attention must be paid to the specific application of the nanoparticles to determine whether adherent particles may or may not have any negative side-effects.

The dilution of particles over time was verified by quantifying the uptake of MLs with different DSTAP contents by TPI-treated cells (Figure 7A); these showed an absence of ML dilution over time in all cases except with MLs containing 16.66% DSTAP (Figure 7B). This finding might be explained by the toxicity of these particles,[20] because uptake levels should be reduced if the particles exhibit cytotoxic effects. Much like CytD, TPI affects tubulin polymerisation and can therefore be considered an effective inhibitor of endocytosis. To avoid inhibition of ML internalisation, the lowest concentration at which TPI efficiently halted cell division was chosen. A slight inhibitory effect was still present, because, for all types of ML used the overall iron content was lower than cells not treated with TPI. However, the effect was not high enough to cause a complete halt to ML dilution over time.

In addition, when 3T3 fibroblasts were incubated with fluorescently labelled MLs containing 3.33% DSTAP, followed by continued culture of these cells in fresh medium not containing MLs, these particles were detectable by fluorescence microscopy in the cells for up to one month postincubation, which is equal to approximately 30 doublings (doubling time: $\pm$20 h; Figure 8). Although 3T3 fibroblasts are known to be highly proliferative cells, this value greatly exceeds the timespan of 5–7 doublings found by Brekke et al.,[33] who used gadolinium rhodamine dextran structures to label Maudsley hippocampal cell clone 36 cells, or by Walczak et al.,[15] who labelled C17.2 neural stem cells with Feridex®. These findings might, however, be somewhat deceiving, because both studies also used fluorescence microscopy to monitor the fate of the internalised nanoparticles over time, but the quantum yield of the label, the amount of fluorophores per particle and the specific cell type used are all parameters that can influence the outcomes of these studies. Nonetheless, these factors could not solely be responsible for the long-term retention of the fluorescent signal of the MLs, which indicates the long persistence of these nanocolloids. The data found here can probably be related to the long-term persistence of the complete ML structure, because single fluorescent lipids or liposomes could not be retained over such long time periods. The long persistence of the label is probably due to the lack of exocytosis and the very high initial iron load of the cell, which greatly exceeds most values described in the literature.[4,26a,34] Furthermore, metabolic processing of the nanoparticles can greatly affect their residence times within cells. Mornet et al.[5] showed that, for the commonly used dextran-coated (U)SPIOs, the dextran coat is degraded within the lysosome, exposing the naked iron oxide core to an acidic environment. Idee et al.[35] also showed that small dextran-coated (U)SPIOs (Sinerem®, 5 nm diameter iron oxide cores) are completely degraded (coating + iron oxide nanocrystal) in the macrophage lysosomal compartment within seven days, which is in line with the rapid loss of the dextran-coated (U)SPIOs mentioned above. During iron oxide metabolism, reactive oxygen species are generated, exposing the cells to stressful conditions.[36] Preliminary results from reduction of nitroblue tetrazolium salts or H_2-DCFDA by cells incubated with our cationic MLs show that the iron oxide cores of the MLs do not induce reactive oxygen species production (data not shown). This further supports our contention that the iron oxide cores are thoroughly shielded by the phospholipid bilayers and thus extremely stable in all aspects. To support these findings, MR experiments to test the persistence of the contrast agents in the MR signal over time are currently being set up, because MR is less sensitive than fluorescence microscopy and other factors, such as the cell density and the number of cells per voxel, must also be taken into consideration.

Conclusions

An interesting feature of MLs is the flexibility of their coatings, which allow easy modification of the lipid constitutions of the bilayers; this results in, for instance, the construction of MLs containing 3.33% DSTAP, which show high labelling efficiency and complete lack of cytotoxic effects.[20] As outlined in this work, fluorescently tagged lipid conjugates can easily be incorporated into either of the ML layers by simple modification of the production procedure; this leads to the generation of bimodal contrast agents. It is demonstrated that MLs are not actively exocytosed and are very stable over time; their retention times greatly exceeded those of the more commonly used (U)SPIOs. This finding supports the use of MLs to improve current contrast-agent enhanced MRI, for which long-term stability of the label would be highly useful in a serial follow-up study of, for instance, cell migration or for monitoring the fate of rapidly dividing cells with high expansion capabilities, such as multipotent adult progenitor cells,[37] after in vivo transplantation—a situation in which other labels, such as the more common dextran-coated particles, cannot be employed effectively because of the rapid loss of label.[15]

Experimental Section

Materials: Dimyristoylphosphatidylcholine (DMPC), dipalmitoylphosphatidylcholine (DPPC) and 1,2-distearoyl-3-trimethylammonium-propane (DSTAP) were purchased from Avanti Polar Lipids (Alabaster, AL, USA). 2-(4,4-Difluoro-5,7-dimethyl-4-bora-3a,4a-diaza-*s*-indacene-3-pentanoyl)-1-hexadecanoyl-*sn*-glycero-3-phosphocholine (β-BODIPY FL C_5-HPC), dipalmitoylphosphatidylethanolamine (DPPE)-Lissamine™ Rhodamine B and DPPE-Texas Red were purchased from Molecular Probes (Invitrogen, Belgium). *N*-Tris(hydroxymethyl)-methyl-2-aminoethanesulfonic acid (TES) and 3-(4,5-dimethylthiazol-2-yl)-2,5-diphenyltetrazolium bromide (MTT) salt were obtained from Sigma (Bornem, Belgium). The disodium salt of 4,5-hydroxybenzene-1,3-disulfonic acid (Tiron) was from Acros Organics (Geel, Belgium). The BCA™ Protein Assay Kit 1296.3, containing reagents A and B, was from Pierce (Rockford, US). Nuclear fast red and potassium ferrocyanide were from Carl Roth (Karlsruhe, Germany). ProLong® Gold anti-fade reagent containing 4′-6-diamidino-2-phenylindole (DAPI) was from Invitrogen (Belgium), and the Lab-Tek™ Chamber Slides™ (Permanox™ slide material, four wells per slide) were from VWR (Belgium). Tubulin polymerisation inhibitor II (TPI) was purchased from Calbiochem (San Diego, USA), and cytochalasin D (Cyt D), nocodazole (Noco), filipin III (Fil), genistein (Gen) and monodansyl cadaverine (MDC) from Sigma–Aldrich. All materials were used as received; the solvents used were pro analysis grade.

Magnetic fluid preparation: Water-adapted dilution-stable magnetite nanoparticles were produced by precipitation of a mixture of Fe^{III} chloride (1 M, 80 mL) and Fe^{II} chloride (2 M, 20 mL) with ammonia (final concentration of 0.7 M). The particles were magnetically decanted and peptised with lauric acid, as described by Khalafalla and Reimers.[9] The stock solution of magnetic fluid had a magnetite content of 114 mg of Fe_3O_4 per mL.

Vesicle preparation: Small unilamellar vesicles were prepared by mixing the desired phospholipid type (183 mg), commonly DMPC (or DPPC for the gas-liquid chromatography experiment), with TES buffer (5 mM, pH 7.0, 15 mL) and sonicating the mixture for 15 min in a temperature-controlled (25 °C) sonication vial at 18 μ peak-to-peak intensity in a probe-tip sonicator (MSE 150 W Ultrasonic Disintegrator, 3/8" sonication probe, Analis, Ghent, Belgium). Any metal particles released by the titanium probe were removed by centrifugation of the dispersion at 7000 g for 10 min.

Magnetoliposome preparation: Neutral MLs were prepared by adding the magnetic fluid described above (0.3 mL) to the small unilamellar vesicles (15 mL) prepared as described above. The vesicle/magnetic fluid mixture was dialysed for three days at 37 °C (SpectraPor no. 2 dialysis tubing, 12–14000 MWCO; Spectrum Laboratories, Medicell Laboratories, London, UK) against TES buffer (5 mM, pH 7.0, 2 L), with a buffer change every 8 h. The resulting MLs were separated from excess vesicles by high-gradient magnetophoresis (HGM; see below). Cationic MLs were produced similarly, but with an additional incubation step (overnight, at 37 °C) of neutral MLs with an equimolar amount (with respect to lipid content) of vesicles containing cationic lipids. Lipids not incorporated in the ML coat were removed by HGM (see below). In practice, to prepare MLs containing DSTAP (3.33%), neutral DMPC MLs were first prepared as described above with an iron oxide concentration of 12.07 mg of Fe_3O_4 per mL and a phosphate concentration of 10.22 μmol of PO_4^{3-} per mL (see below). To prepare cationic vesicles equimolar with respect to lipid content to the neutral MLs, TES buffer (5 mM, pH 7.0, 3 mL) was added to DMPC (18.73 mg) and DSTAP (2.16 mg; that is, 90 and 10 mol% of 30.66 μmol PO_4^{3-}, respectively), and the suspension was sonicated at an 18 μ peak-to-peak intensity in a probe-tip sonicator (MSE 150 W Ultrasonic Disintegrator, exponential sonication probe, Analis, Ghent, Belgium) for 15 min with cooling in ice-cold water. Next, the vesicle suspension (1.5 mL) was mixed with the neutral MLs (1.5 mL), and the mixture was incubated, overnight, at 37 °C, followed by a second round of HGM purification to provide the MLs containing 3.33% DSTAP. Fluorescently tagged MLs containing DSTAP (3.33%) were produced in a similar fashion to the cationic MLs, with the incorporation of β-BODIPY FL C_5-HPC, DPPE-Lissamine™ Rhodamine B or DPPE-Texas Red. The β-BODIPY FL lipid conjugates were located in the inner leaflet of the ML coat, whereas DPPE-Lissamine™ Rhodamine B and DPPE-Texas Red were embedded in the outer layer. The procedures used to generate these structures were as follows:

1) Cationic MLs grafted with a single type of fluorescent lipid conjugate (either DPPE-Lissamine™ Rhodamine B or DPPE-Texas Red) in the outer lipid layer (Scheme 1 A) were produced in a similar way to nonfluorescent cationic MLs (see above), except that the neutral MLs were incubated with cationic vesicles containing the appropriate percentage of fluorescent lipid conjugate (three times the desired percentage of fluorescent label in the ML coat).
2) MLs with a fluorescent lipid conjugate in the inner lipid layer were produced by mixing 3 mL of sonicated vesicles (12 mg of lipids, of which 1 mol% consisted of β-BODIPY FL C_5-HPC) with the magnetic fluid (0.3 mL) at room temperature (Fe_3O_4 concentration of the stock solution: 114 mg mL^{-1}), followed by dialysis (6 h) at 37 °C against TES buffer (5 mM, pH 7.0), with a buffer change every 2 h (Scheme 1 B). Under these conditions all phospholipid components are adsorbed as a single layer on to the magnetite surface.[23] The monolayered MLs were then mixed with DMPC vesicles (12 mL, 171 mg of lipids) and dialysed against TES buffer (5 mM, pH 7.0) for a further two days at 37 °C; this resulted in the formation of the outer lipid layer (Scheme 1 B, 2nd row). After HGM, these MLs were incubated

with cationic vesicles to produce cationic MLs as described above (Scheme 1 B1).

3) MLs containing a different fluorescent lipid conjugate in each of the lipid layers were produced as described in (2), apart from the addition of DPPE-Lissamine™ Rhodamine B (0.75%) to the cationic vesicles; this resulted in cationic MLs bearing DPPE-Lissamine™ Rhodamine B (0.25%; Scheme 1 B2). Because intramembrane flip-flop movements are believed to occur at a very slow rate (see Discussion), the inner lipid layer contains only β-BODIPY FL C_5-HPC, whereas the outer layer contains only DPPE-Lissamine™ Rhodamine B.

The integrity of the lipid bilayer of each ML sample was tested by iron and phosphate determination, as described previously.[20] The procedure for transmission electron microscopy (TEM) for visualisation of the magnetic fluid grains, cationic MLs and cell-internalised MLs is outlined in the Supporting Information.

High-gradient magnetophoresis: Separation of MLs from excess lipids was achieved by HGM, in which magnetisable stainless steel fibres were inserted into sections of tubing (Medical grade Silastic tubing, length 10 cm, inner and outer diameters of 0.02 and 0.32 cm, respectively, Dow–Corning Corporation) positioned between the poles of a working electromagnet (Bruker B-E 15, Karlsruhe, Germany) operating at a magnetic field of 1.5 T. Aliquots (0.75 mL) of the samples were pumped through the magnetic filter device by use of a peristaltic pump (proportioning pump, Model 1512/20, Carlo Erba, Italy), followed by being washed with TES buffer (5 mM, pH 7.0, 0.75 mL). After deactivation of the magnet, the trapped particles were eluted from the filter with the desired volume of the same buffer.

Quantification of fatty acyl moieties: DPPC-MLs were incubated with an equimolar amount (with respect to lipid content) of DMPC/DSTAP (80:20) vesicles at room temperature. At several time points, samples were taken and subjected to HGM purification, both the retentate and eluate being collected. Time-dependent changes in the fatty acyl composition of the membranes were monitored by gas-liquid chromatography (Mega 8180-O, Carlo Erba, Rodano, Italy). For this purpose, the phospholipids were subjected to acid hydrolysis and their fatty acids were converted into the more volatile methyl esters by use of acetyl chloride (10%) in methanol.[38] Heptadecanoic acid was used as internal standard.

Electrophoretic mobility measurements: The electrophoretic mobility was measured with a Zetasizer IIC instrument (Malvern, UK) at 25 °C. Immediately prior to measurement, the samples were diluted with TES buffer (5 mM, pH 7.0) to optimise the response of the machine for the given sample. The average value of ten different runs was then calculated.

Statistical analysis: Unless indicated otherwise, values are represented as the mean ± standard error of the mean (SEM). For cell viability, cellular iron content and relative fluorescence intensities, direct comparisons between two conditions were performed by use of the unpaired Student's t-test, and the degree of significance is given when appropriate (*: $p < 0.05$; **: $p < 0.01$; ***: $p < 0.001$).

Cell culturing conditions and detailed information on the different magnetoliposome–cell interaction experiments are described in the Supporting Information.

Acknowledgements

Electron microscopy was performed by Prof. Johan Baert (Laboratory of Histology, KULeuven–Campus Kortrijk). N2a and HEK-293 cells were a kind gift from Evelyne Coussée (Laboratory of Physiology, KULeuven–Campus Kortrijk), and Geneswitch™-CHO and HUVECs were kindly provided by Prof. Karen Vanhoorelbeke (Laboratory of Thrombosis Research, KULeuven–Campus Kortrijk). S.J.H.S. and D.V. are recipients of research grants from the Institute for the Promotion of Innovation through Science and Technology in Flanders (IWT–Vlaanderen). M.D.C. is a recipient of a IWT grant (StrategischBasisOnderzoek), sponsoring project no. 80017 entitled "Integrated magnetic nanoparticle-enabled imaging of therapeutic cells"—"iMAGiNe".

Keywords: cell labeling · colloids · imaging agents · magnetoliposomes · nanostructures

[1] F. Scherer, M. Anton, U. Schillinger, J. Henke, C. Bergemann, A. Krüger, B. Gänsbacher, C. Planck, *Gene Ther.* **2002**, *9*, 102–109.
[2] a) A. Ito, H. Honda, T. Kobayashi, *Cancer Immunol. Immunother.* **2006**, *55*, 320–328; b) J.-P. Fortin, C. Wilhelm, J. Servais, C. Ménager, J.-C. Bacri, F. Gazeau, *J. Am. Chem. Soc.* **2007**, *129*, 2628–2635.
[3] a) J. W. M. Bulte, T. Douglas, B. Witwer, S. Zhang, E. Strable, B. Lewis, H. Zywicke, B. Miller, P. van Gelderen, B. Moskowitz, I. Duncan, J. Frank, *Nat. Biotechnol.* **2001**, *19*, 1141–1147; b) M.-S. Martina, J.-P. Fortin, C. Ménager, O. Clément, G. Barrat, C. Grabielle-Madelmont, F. Gazeau, V. Cabuil, S. Lesieur, *J. Am. Chem. Soc.* **2005**, *127*, 10676–10685.
[4] C. Berry, A. Curtis, *J. Phys. D* **2003**, *36*, R198–R206.
[5] S. Mornet, S. Vasseur, F. Grasset, E. Duguet, *J. Mater. Chem.* **2004**, *14*, 2161–2175.
[6] a) E. M. Shapiro, S. Skrtic, K. Sharer, J. Hill, C. Dunbar, A. Koretsky, *Proc. Natl. Acad. Sci. USA* **2004**, *101*, 10901–10906; b) A. Gupta, M. Gupta, *Biomaterials* **2005**, *26*, 3995–4021.
[7] M. Hoehn, E. Küstermann, J. Blunk, D. Wiedermann, T. Trapp, S. Wecker, M. Föcking, H. Arnold, J. Hescheler, B. Fleischmann, W. Schwindt, C. Bührle, *Proc. Natl. Acad. Sci. USA* **2002**, *99*, 16267–16272.
[8] a) A. Norman, S. Thomas, R. Pratt, S. Lu, R. Norgren, *Brain Res.* **1992**, *594*, 279–283; b) S. J. H. Soenen, M. Hodenius, T. Schmitz-Rode, M. De Cuyper, *J. Magn. Magn. Mater.* **2008**, *320*, 634–641.
[9] S. E. Khalafalla, G. W. Reimers, *IEEE Trans. Magn.* **1980**, *16*, 178.
[10] M. De Cuyper, M. Joniau, *Eur. Biophys. J.* **1988**, *15*, 311–319.
[11] S. Mornet, J. Portier, E. Duguet, *J. Magn. Magn. Mater.* **2005**, *293*, 127–134.
[12] E. Groman, L. Josephson, US patent No. 5248492 (, **1993**).
[13] a) L. Josephson, C. Tung, A. Moore, R. Weissleder, *Bioconjugate Chem.* **1999**, *10*, 186–191; b) C. Kaufman, M. Williams, L. Ryle, T. Smith, M. Tanner, C. Ho, *Transplantation* **2003**, *76*, 1043–1046.
[14] M. Babincová, V. Altanerova, C. Altaner, P. Čičmanec, P. Babinec, *Med. Phys.* **2004**, *31*, 2219–2221.
[15] P. Walczak, D. A. Kedziorek, A. A. Gilad, B. P. Barnett, J. W. M. Bulte, *Magn. Reson. Med.* **2007**, *58*, 261–269.
[16] B. L. Strand, T. L. Ryan, P. In't Veld, B. Kulseng, A. M. Rokstad, G. Skjak-Brek, T. Espevik, *Cell Transplant.* **2001**, *10*, 263–275.
[17] V. A. P. Garcia, L. M. Lacava, S. Kückelhaus, R. B. Azevedo, M. Da Silva, P. C. Morais, M. De Cuyper, Z. G. M. Lacava, *Eur. Cell Mater.* **2002**, *3 (Suppl. 2)*, 154–155.
[18] M. De Cuyper, D. Caluwier, J. Baert, J. Cocquyt, P. Van der Meeren, *Z. Phys. Chem.* **2006**, *220*, 133–141.
[19] a) M. De Cuyper, A. Crabbe, J. Cocquyt, P. Van der Meeren, F. Martins, M. Santana, *Phys. Chem. Chem. Phys.* **2004**, *6*, 1487–1492; b) M. De Cuyper, S. J. H. Soenen, K. Coenegrachts, L. Ter Beek, *Anal. Biochem.* **2007**, *367*, 266–273.
[20] S. J. H. Soenen, J. Baert, M. De Cuyper, *ChemBioChem* **2007**, *8*, 2067–2077.
[21] V. Kanchan, A. Panda, *Biomaterials* **2007**, *28*, 5344–5357.

[22] M. De Cuyper, M. Joniau, H. Dangreau, *Biochemistry* **1983**, *22*, 415–420.
[23] M. De Cuyper, M. Joniau, *Langmuir* **1991**, *7*, 647–652.
[24] A. Papadopulos, S. Vehring, I. López-Montero, L. Kutschenko, M. Stöckl, P. Devaux, M. Kozlov, T. Pomorski, A. Herrmann, *J. Biol. Chem.* **2007**, *282*, 15559–15568.
[25] F. Krötz, C. de Wit, H. Y. Sohn, S. Zahler, T. Gloe, U. Pohl, C. Planck, *Mol. Ther.* **2003**, *7*, 700–710.
[26] a) J. W. M. Bulte, S. Zhang, P. van Gelderen, V. Herynek, E. K. Jordan, I. D. Duncan, J. Frank, *Proc. Natl. Acad. Sci. USA* **1999**, *96*, 15256–15261; b) P. Jendelová, V. Herynek, L. Urdzíková, K. Glogarová, J. Kroupová, B. Andersson, V. Bryja, M. Burian, M. Hájek, E. Syková, *J. Neurosci. Res.* **2004**, *76*, 232–243.
[27] J. Panyam, V. Labhasetwar, *Pharm. Res.* **2003**, *20*, 212–220.
[28] C. Gonçalves, E. Mennesson, R. Fuchs, J.-P. Gorvel, P. Midoux, C. Pichon, *Mol. Ther.* **2004**, *10*, 373–385.
[29] M. Piper, S. Salih, C. Weinl, C. Holt, W. Harris, *Nat. Neurosci.* **2005**, *8*, 179–186.
[30] A. Subtil, I. Gaidarov, K. Kobylarz, A. Lampson, J. Keen, T. McGraw, *Proc. Natl. Acad. Sci. USA* **1999**, *96*, 6775–6780.
[31] J. Rejman, V. Oberle, I. Zuhorn, D. Hoekstra, *Biochem. J.* **2004**, *377*, 159–169.
[32] a) K. Hinds, J. Hill, E. M. Shapiro, M. Laukkanen, A. Silva, C. Combs, T. Varney, R. Balaban, A. Koretsky, C. Dunbar, *Blood* **2003**, *102*, 867–872; b) A. Arbab, L. Wilson, P. Ashari, E. Jordan, B. Lewis, J. Frank, *NMR Biomed.* **2005**, *18*, 383–389.
[33] C. Brekke, S. Morgan, A. Lowe, T. Meade, J. Price, S. Williams, M. Modo, *NMR Biomed.* **2007**, *20*, 77–89.
[34] P. Jendelová, V. Herynek, J. DeCroos, K. Glogarová, B. Andersson, M. Hájek, E. Syková, *Magn. Reson. Med.* **2003**, *50*, 767–776.
[35] J.-M. Idee, M. Port, I. Raynal, M. Schaefer, B. Bonemain, P. Prigent, P. Robert, C. Robic, C. Corot in *Nanotechnologies for the Life Sciences, Vol. 10* (Ed.: C. Kumar), Wiley-VCH, Weinheim, **2007**, chapter 2.
[36] J. W. M. Bulte, A. Arbab, T. Douglas, J. Frank, *Methods Enzymol.* **2004**, *386*, 275–299.
[37] M. Reyes, S. Li, E. Kimura, L. Meuse, J. Chamberlain, *Mol. Ther.* **2004**, *9*, S145.
[38] W. W. Christie, *Gas Chromatography and Lipids: A Practical Guide*, 1st ed., Oily Press Ltd., Alloway, **1990**.

Received: July 28, 2008
Published online on December 12, 2008

